EUROGRAPHICS 2013 / I. Navazo, P. Poulin
(Guest Editors)

*Volume 32 (2013), Number 2*

# Landmark-Guided Elastic Shape Analysis of Spherically-Parameterized Surfaces

Sebastian Kurtek[1], Anuj Srivastava[2], Eric Klassen[3], and Hamid Laga[4]

[1] Dept. of Statistics, Ohio State University, [2] Dept. of Statistics, Florida State University,[3] Dept. of Mathematics, Florida State University,
[4] Phenomics and Bioinformatics Research Centre, University of South Australia

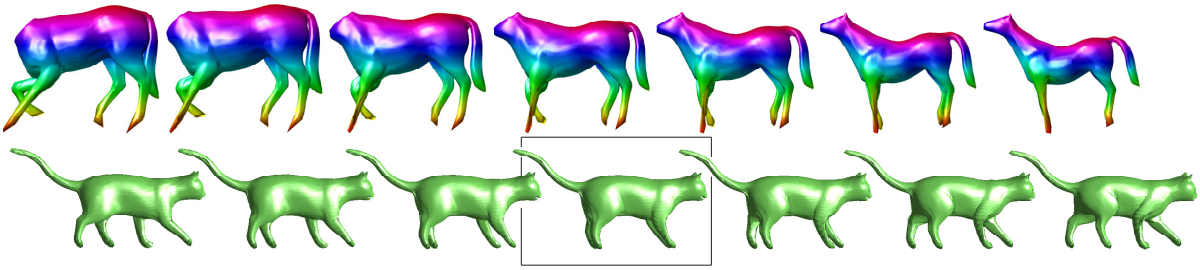

**Figure 1:** *Top: Geodesic path between two surfaces with missing parts. Our approach can compute dense correspondences (illustrated with matching colors) and geodesics efficiently. Bottom: symmetrization of a highly articulated shape. The length of the geodesic provides a measure of asymmetry of the shape. Its mid-point is a symmetric version of the initial shape.*

**Abstract**

*We argue that full surface correspondence (registration) and optimal deformations (geodesics) are two related problems and propose a framework that solves them simultaneously. We build on the Riemannian shape analysis of anatomical and star-shaped surfaces of Kurtek et al. and focus on articulated complex shapes that undergo elastic deformations and that may contain missing parts. Our core contribution is the re-formulation of Kurtek et al.'s approach as a constrained optimization over all possible re-parameterizations of the surfaces, using a sparse set of corresponding landmarks. We introduce a landmark-constrained basis, which we use to numerically solve this optimization and therefore establish full surface registration and geodesic deformation between two surfaces. The length of the geodesic provides a measure of dissimilarity between surfaces. The advantages of this approach are: (1) simultaneous computation of full correspondence and geodesic between two surfaces, given a sparse set of matching landmarks (2) ability to handle more comprehensive deformations than nearly isometric, and (3) the geodesics and the geodesic lengths can be further used for symmetrizing 3D shapes and for computing their statistical averages. We validate the framework on challenging cases of large isometric and elastic deformations, and on surfaces with missing parts. We also provide multiple examples of averaging and symmetrizing 3D models.*

Categories and Subject Descriptors (according to ACM CCS): I.3.5 [Computer Graphics]: Computational Geometry and Object Modeling—Boundary Representations;

## 1. Introduction

Finding correspondences (registration) between surfaces, and finding *natural* deformations (geodesics) that align 3D objects to one another, referred to as shape analysis, are fundamental problems in computer graphics [OLGM11, YYPM11, ACP03]. Many shape processing and 3D modeling applications require the alignment of shapes that differ not only in tessellation and pose but also undergo large elastic deformations and contain missing parts. Previous geodesic computation techniques assume that the shapes are

already in full correspondence while restricting their deformations to being isometric [KMP06, HRWW12]. Full correspondences are either manually specified or computed separately [vKZHCO10] in a pre-processing step. The cost functions used for registration are often unrelated to those used for shape comparisons and deformations.

We put forward the idea that optimal surface registration and computation of geodesic paths between surfaces are two related problems that we solve simultaneously in a unified Riemannian framework. We focus on genus-0 surfaces that undergo complex isometric and elastic deformations and may contain missing parts. An important issue is to choose a Riemannian metric that results in semantically plausible registrations and geodesics. Srivastava et al. [SKJJ11] and Kurtek et al. [KKG*12, KKD*11b] developed Riemannian metrics and used them in fully automated frameworks for the analysis of curves, and anatomical and star-shaped genus-0 surfaces. Their methods fail to produce globally optimal solutions when dealing with complex and heavily articulated shapes as shown in Fig. 2. While fully automated solutions are desirable, matching human registration, when dealing with complex shape deformations, is challenging. Thus, it is reasonable to argue that no metric is able to produce registrations that result in semantically correct geodesics across general surfaces without incorporating a-priori semantic knowledge. On the other hand, assuming the availability of a dense correspondence, as in [KMP06, HRWW12], is not practical for large and complex shapes.

We propose a framework that can use additional information, in the form of registered coarse landmarks, to simultaneously compute dense correspondences and geodesics between complex surfaces. A sparse set of landmarks can be easily detected by looking at shape extremities or regions of high Gaussian curvature, or manually selected, which is highly desirable in applications such as motion and performance capture, attribute transfer, or medical imaging. We formulate the joint registration and geodesic computation as a *constrained* optimization over all possible reparameterizations of surfaces. The advantage of this formulation is two-fold; first, using only few landmark correspondences, typically four to ten, we are able to find dense correspondences and deformations (without relying upon shape descriptors) between complex shapes that undergo large isometric or elastic deformations, and in the presence of missing parts. Second, the proposed approach provides actual deformations (geodesics) and proper distances (geodesic lengths), which we further use for symmetry analysis of shapes, and for computing average shapes.

**Related work.** Computing geodesics between surfaces consists of finding an optimal deformation that takes one surface to another. The challenging question is of defining the optimality criterion. One solution is to use geodesic distances under a chosen Riemannian metric on the space of objects. This provides a proper distance for use in shape comparison and shape statistics (e.g. mean shapes and covariance). Motivated by the progress in shape analysis of curves [YMS*08, SKJJ11], there have been several recent papers that compute geodesic-based deformations of surfaces under a Riemannian metric [BGK95, KMP06, HRWW12]. They assume that the surfaces undergo nearly isometric deformations and that they are already in full correspondence, which is very limiting. Thus, these methods provided only part of the desired solution. Our approach simultaneously solves for dense correspondences and geodesics, and handles a larger class of deformations, including large elastic deformations.

Common approaches to finding dense correspondences [vKZHCO10] are based on matching feature points using geometric descriptors. Others conformally embed the surfaces to a canonical domain, then find the best Möbius transform that aligns the two domains [LF09, ZWW*10]. These approaches are limited to (nearly) isometric deformations. Others considered elastic deformations [ZSCO*08, WSSC11a, WSSC11b, KLF11]. Kim et al. [KLF11] focused on genus-0 surfaces. They use a weighted combination of maps produced by Möbius voting. The produced "blended" map can then be used to construct deformation paths (geodesics) by interpolating registered pairs of points [WSSC11a], often using an optimality criterion that is different from the one used for computing the correspondences. The inter-surface maps produced by these methods are not guaranteed to be a diffeomorphism and thus the constructed geodesics are not natural and exhibit several artifacts and distortions as shown in Fig. 7. To the best of our knowledge, [KKG*12] was the first paper to study registration, deformation, and comparison of surfaces in a unified Riemannian framework. The approach works on anatomical and star-shaped surfaces, but fails to find correct dense correspondences and plausible geodesics when the shapes are heavily articulated, unlike the solution we propose. The use of anatomical landmarks has been previously suggested for registration, but does not lead to proper metrics for shape comparison as we do in this paper.

Finally, shape morphing is a well studied problem. However most of the existing techniques [KS04] do not provide a proper metric that can be used for shape analysis as we do in this paper.

**Overview and contributions.** We take as input two triangulated meshes with a sparse set of corresponding landmarks (typically four to ten). First, we spherically parameterize the two meshes. Then, in a joint Riemannian framework, we solve for a dense correspondence and a geodesic between them. The length of the geodesic, which is a proper distance as it satisfies symmetry, positive definiteness, and triangle inequality, provides a measure of similarity between the two surfaces. Our approach can handle large elastic deformations between heavily articulated shapes, which may also contain missing parts as shown in Fig. 1.

We build on a collection of existing pieces and reach an

efficient, comprehensive system that is more than the sum of its parts in performance. The first component is the definition of a shape space and a Riemannian metric on this space (Sec. 2). Geodesics in this space correspond to optimal and natural deformations that align one shape onto another. Kurtek et al. [KKD*11b, KKDS10, KKG*12] solve the registration problem as an optimization over all possible rotations and re-parameterizations of surfaces. Our core contribution is the re-formulation of this approach as a *constrained* optimization using a sparse set of automatically detected or manually specified corresponding landmarks (Sec. 3). Unlike [KKG*12], which studied only simple anatomical structures, our framework can handle complex shapes since it gets closer to the global optimum when performing the registration step. To numerically solve this constrained optimization problem, we introduce a landmark-constrained basis of smooth, tangent vector fields that vanish at the landmarks (Sec. 3.2). This formulation enables the preservation of the nice mathematical properties of the Riemannian framework, such as proper geodesic distances and geodesic deformations, without the need for specifying dense correspondences. We also introduce an initialization step that finds an initial diffeomorphic mapping of surfaces using the sparse set of landmarks (Sec. 2.1). Our contributions are:

1. An efficient implementation of the spherical parameterization of 3D meshes [PH03], which we constrain to map landmarks on $\mathbb{S}^2$ to given landmarks on the meshes.
2. A joint solution to the correspondence and geodesic problems using only a sparse set of landmarks, extending [KKG*12] that cannot handle heavily articulated shapes and overcoming the limitations of [KMP06, HRWW12], which assume full correspondences as given.
3. The preservation of nice mathematical properties, such as proper geodesic distances and geodesic deformations, despite the presence of the additional landmark constraints.
4. A definition of a landmark-constrained basis used to numerically solve the constrained correspondence problem.
5. We demonstrate the efficiency of our framework on a collection of highly articulated shapes that undergo large elastic deformations and contain missing parts (Sec. 4). To the best of our knowledge, this is the first time that such a comprehensive set of results is presented.
6. We extend the framework to computing averages of complex shapes, an important step towards building shape atlases, and to shape symmetrization. We show that the proposed metric provides a measure of asymmetry of shapes.

## 2. Surface Representation and Metric

We are interested in simultaneously solving the problem of registration and deformation (using geodesics) between highly articulated spherical surfaces. Let the set of all such surfaces be $\mathcal{F} = \{f : \mathbb{S}^2 \mapsto \mathbb{R}^3 | \int_{\mathbb{S}^2} |f(s)|^2 ds < \infty$ and $f$ is smooth$\}$, where $ds$ is the standard Lebesgue measure on $\mathbb{S}^2$, and $|\cdot|$ denotes the standard 2-norm in $\mathbb{R}^3$. (In case points on $\mathbb{S}^2$ are expressed in spherical coordinates $s = (\theta, \phi)$, then $ds$ is given by $\sin(\theta) d\theta d\phi$.) Also, let $\Gamma$ be the set of all diffeomorphisms of $\mathbb{S}^2$ to itself. Let each surface of interest be annotated, either automatically or manually, by a small number ($n$) of landmarks. Let $s_1, s_2, \ldots, s_n$ be standardized locations of these landmarks on $\mathbb{S}^2$, such that $f(s_i)$, $i = 1, 2, \ldots, n$ become the given landmarks on a parametrized surface $f$. We will assume that for any two surfaces $f_1$ and $f_2$, the corresponding landmark pairs are $\{f_1(s_i), f_2(s_i)\}$. The automatic detection and matching of landmarks will be discussed in Section 3.4. Now, we define $\Gamma_0 = \{\gamma \in \Gamma | \gamma(s_i) = s_i,\ i = 1, 2, \ldots, n\} \subset \Gamma$. $\Gamma_0$ will act as the reparametrization group for spherically embedded surfaces.

It has been shown in previous work [KKDS10] that endowing $\mathcal{F}$ with the $\mathbb{L}^2$ metric does not result in a proper framework for comparing shapes of parameterized surfaces, for several reasons: the registration $\min_\gamma \|f_1 - f_2 \circ \gamma\|$ can lead to a *pinching* of parts of $f_2$, the resulting registration is not symmetric in $f_1$ and $f_2$, and the re-parameterization group does not act by isometries under this metric, i.e. $\|f_1 \circ \gamma - f_2 \circ \gamma\| \neq \|f_1 - f_2\|$. Thus, in this paper we take an alternative approach proposed by Kurtek et al. [KKDS10, KKD*11b, KKG*12]. We provide some of the details next. Let $f_x(s)$ and $f_y(s)$ denote partial derivatives at the point $s = (x, y) \in \mathbb{S}^2$. To define a Riemannian metric on $\mathcal{F}$, we use the following representation of surfaces:

**Definition 1** Define the mapping $Q : \mathcal{F} \to \mathbb{L}^2$ as $Q(f)(s) = q(s) = \sqrt{|a(s)|} f(s)$, where $|a(s)| = |f_x(s) \times f_y(s)|$ is the area of $f$ at $s \in \mathbb{S}^2$. $q$ is called the $q$-map of the surface $f$.

The set of all $q$-maps is a subset of $\mathbb{L}^2$. If a surface $f$ is re-parameterized to $f \circ \gamma$, $\gamma \in \Gamma_0$, then the corresponding $q$-map is changed to $(q, \gamma) = \sqrt{J_\gamma}(q \circ \gamma)$, where $J_\gamma$ is the Jacobian of $\gamma$. Note that re-parameterization of surfaces is exactly the same as the registration problem. In other words, the search for optimal correspondence is actually performed by optimally re-parameterizing the given surfaces, while maintaining landmark correspondences.

Kurtek et al. [KKD*11b] chose the natural $\mathbb{L}^2$ metric on the space of $q$-maps. This choice has the advantage that the $\mathbb{L}^2$ distance between $q$-maps of surfaces is preserved under identical re-parameterizations. That is, if $q_1$ and $q_2$ are $q$-maps of any two surfaces, then $\|q_1 - q_2\| = \|(q_1, \gamma) - (q_2, \gamma)\|$ for any $\gamma \in \Gamma$. This property is important in solving the registration problem and at the same time obtaining a proper distance. The Riemannian metric that is used on $\mathcal{F}$ is the pullback of the $\mathbb{L}^2$ metric from that space. Let $\langle\langle \cdot, \cdot \rangle\rangle$ denote the Riemannian metric on $\mathcal{F}$, and let $T_f(\mathcal{F})$ be the tangent space of $\mathcal{F}$ at $f$. With this induced metric, $\mathcal{F}$ becomes a Riemannian manifold and one wants to compute geodesic distances between two points, say $f_1$ and $f_2$, in $\mathcal{F}$.

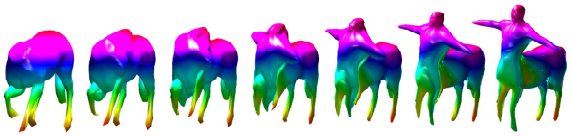

**Figure 2:** *A geodesic between objects undergoing elastic deformations and containing missing parts generated with the approach in [KKG*12]. The quality of the geodesic is very poor compared to our approach (see Fig. 4-(b)).*

### 2.1. Initial Registration Using Landmarks

As a first step in our approach we must find two initial diffeomorphisms $\gamma_1,\ \gamma_2 : \mathbb{S}^2 \to \mathbb{S}^2$ that map the selected landmarks on surfaces $f_1$ and $f_2$ with locations $(\tilde{s}_1,\ldots\tilde{s}_n \in \mathbb{S}^2)$ and $(\bar{s}_1,\ldots\bar{s}_n \in \mathbb{S}^2)$, respectively, to the standard landmarks $(s_1,\ldots,s_n \in \mathbb{S}^2)$. We describe the procedure of finding $\gamma_1$ and note that $\gamma_2$ can be found in the same manner.

Although we do not require any optimal property associated with $\gamma_1$, it does make sense to seek a diffeomorphism that is optimal in the sense of a quadratic deformation energy, similar to splines on Euclidean spaces. However, since the deformations between the landmarks can be very large, one cannot directly construct the deformation maps by integration of velocity fields that minimize a quadratic smoothness energy under the specified landmark constraints, as in [GVM04]. Instead, we take a different approach. We divide the problem into $k$ smaller deformation steps and proceed as follows; we connect each pair of matched landmarks on $\mathbb{S}^2$ with a great circle and sample it uniformly using $k$ steps. Then, we solve for a small deformation that matches the $(k-1)st$ point to the $k$th point on this circle for all $j$: let $\alpha_j$ be the tangent (shooting) vector to $\mathbb{S}^2$ at $\tilde{s}_j$ such that $\exp_{\tilde{s}_j}(\alpha_j) = s_j$. Then, using a reproducing kernel $K$ on $\mathbb{S}^2$, define a vector field on $\mathbb{S}^2$ according to $s \mapsto V_s \equiv \sum_{j=1}^n K(s,s_j)\alpha_j$ in such a way that $V_{s_j} = \alpha_j$. The desired deformation mapping is obtained by computing $s \mapsto \exp_s(V_s)$. A composition of these $k$ small deformations leads to the larger desired deformation $\gamma_1$.

### 2.2. Pre-Shape and Shape Space

Given that the landmarks across the two surfaces are now matched, we start by normalizing the translation and scale of the two surfaces. First, we translate them such that their centers of mass are at the origin and then scale them to have unit area. With a slight abuse of notation, we re-define $\mathcal{F}$ as the space of normalized surfaces and will refer to it as the pre-shape space. The remaining groups, i.e. rotation and constrained re-parameterization, are dealt with differently, by removing them algebraically from the representation space. Note that specifying fixed landmarks on a surface does not change the rotation group, but it constrains the re-parameterization group to a subgroup that fixes the landmarks. The rotation group $SO(3)$ acts on $\mathcal{F}$, $SO(3)\times\mathcal{F}\to\mathcal{F}$ according to $(O,f) = Of$. The constrained re-parameterization group $\Gamma_0$ acts on $\mathcal{F}$, $\mathcal{F}\times\Gamma_0\to\mathcal{F}$ with $(f,\gamma) = (f\circ\gamma)$. Then, an equivalence class of a surface $f$ is given by $[f] = \text{closure}\{O(f\circ\gamma)|O\in SO(3),\gamma\in\Gamma_0\}$ and represents a shape with fixed landmarks uniquely. The set of all such equivalence classes is defined to be $\mathcal{S}$, the *shape space*. Because $SO(3)\times\Gamma_0$ acts on $\mathcal{F}$ by isometries the metric descends to the quotient space $\mathcal{S}$ making it a metric space.

With this formulation, the registration of two surfaces becomes a search for the optimal rotation $O$ and re-parameterization $\gamma\in\Gamma_0$. The shape space $\mathcal{S}$, however, is different from prior papers in that the subgroup $\Gamma_0$ is being considered here, instead of the full $\Gamma$. This poses additional difficulties when exploring this space. In particular, the search space becomes disconnected and the search for an optimal solution with gradient descent-like techniques may require multiple initializations for finding the global optimum. Assuming that the initial diffeomoprhic registration of surfaces, obtained using landmarks as described in the previous section, is in the optimal subset, we can restrict our search for optimal incremental diffeomorphisms to only the subset that contains the identity map. Since this subset is connected, the gradient-based search is sufficient for our application.

### 2.3. Geodesic Computation

We start with two spherically parameterized surfaces $f_1$ and $f_2$, such that $f_j(s_i)$, $i = 1,2,\ldots,n$, and $j = 1,2$, denote the landmarks on them. We define the geodesic distance in $\mathcal{S}$ between $f_1$ and $f_2$, denoted $d([f_1],[f_2])$, as follows:

$$\min_{\gamma\in\Gamma_0, O\in SO(3)} \left( \min_{\substack{F:[0,1]\to\mathcal{F} \\ F(0)=f_1,\ F(1)=O(f_2\circ\gamma)}} \left( \int_0^1 \langle\langle F_t(t), F_t(t)\rangle\rangle^{(1/2)}\, dt \right) \right), \tag{1}$$

where $F(t)$ is a parameterized path in $\mathcal{F}$. The quantity $L[F] = \int_0^1 \langle\langle F_t(t), F_t(t)\rangle\rangle^{(1/2)}\, dt$ denotes the length of $F$. The inside minimization refers to finding the shortest path (geodesic) between $f_1$ and $O(f_2\circ\gamma)$ in $\mathcal{F}$, which can be solved using a path-straightening algorithm. This algorithm has been previously used to find geodesics between closed curves [SKJJ11] and simple star-shaped surfaces [KKG*12]. The basic idea behind this algorithm is to iteratively update the path according to a gradient of an energy, which is closely related to the length of this path. A critical point of this energy results in a geodesic path and distance between $f_1$ and $f_2$ under given rotations and parameterizations, referred to as $d_{\mathcal{F}}$. The outside minimization problem computes the full correspondence, i.e., registration between $f_1$ and $f_2$, which is a search over $SO(3)\times\Gamma_0$. The fact that $d_{\mathcal{F}}$ is a proper distance comes from the fact that $\Gamma_0$ acts on $\mathcal{F}$ by isometries. The resulting geodesic in $\mathcal{S}$ is denoted with $F^*$.

## 3. Landmark-Constrained Correspondence

The outside minimization in Eqn. 1 is a search over $SO(3) \times \Gamma_0$. The solution is iterative where one alternates between computing the optimal rotation $O \in SO(3)$ given a fixed parameterization, and computing the optimal parameterization $\gamma^*$ given a fixed rotation. One can perform these optimizations over the geodesic path length, as suggested in Eqn. 1. Instead, we will solve this registration problem using the $\mathbb{L}^2$ norm between the $q$-map representations of the two surfaces, in order to greatly simplify computations. We provide more details next.

### 3.1. Optimization over $SO(3) \times \Gamma$:

Given two surfaces $f_1$ and $f_2$ with fixed parameterizations we first compute their corresponding $q$-maps, $q_1$ and $q_2$. Then, the optimal rotation is computed using the Procrustes method. Compute the $3 \times 3$ matrix $A = \int_{\mathbb{S}^2} q_1(s) q_2(s)^T ds$. Using the singular value decomposition $A = U\Sigma V^T$, we can define the optimal rotation as $O^* = UV^T$ (if the determinant of $A$ is negative the last column of $V^T$ changes sign).

Given a fixed rotation, the optimization problem over $\Gamma_0$ is solved using a gradient descent approach based on the following energy: $E_{\gamma_{id}}(\gamma) = \|q_1 - \phi_{q_2}(\gamma)\|^2$, where $\phi_{q_2}(\gamma) = (q_2 \circ \gamma)\sqrt{J_\gamma}$. Since $\gamma$ is infinite-dimensional, we express the gradient of $E$ with respect to $\gamma$ using a basis of $T_{\gamma_{id}}(\Gamma_0)$, the tangent space of $\Gamma_0$ at $\gamma_{id}$. The directional derivative of $E$ in a direction $b$ is given by $\langle q_1 - \phi_{q_2}(\gamma_{id}), \phi_{*,\gamma_{id}}(b)\rangle b$, where $\phi_{*,\gamma_{id}}$ is the differential of $\phi$. Given an orthonormal basis $\{b_i\}$ for $T_{\gamma_{id}}(\Gamma_0)$ we can estimate the gradient of $E$ using $\nabla E \approx \sum_{i=1}^m \langle q_1 - \phi_{q_2}(\gamma_{id}), \phi_{*,\gamma_{id}}(b_i)\rangle b_i$ and update the current estimate of the optimal parameterization according to this gradient. Since the gradient $\nabla E$ is a tangent vector field on $\mathbb{S}^2$, the update is performed by mapping the point $s \in \mathbb{S}^2$ according to $s \mapsto (\cos(\varepsilon\theta(s))s + \frac{\sin(\varepsilon\theta(s))}{\theta(s)}\nabla E(s))$, where $\theta(s) = |\nabla E(s)|$ and $\varepsilon$ is the step size.

### 3.2. Landmark-Constrained Basis

To solve the optimization problem over $\Gamma_0$ we need to define a set of tangent, smooth vector fields that vanish at the landmarks $s_i \in \mathbb{S}^2$. These vector fields form an orthonormal basis for $T_{\gamma_{id}}(\Gamma_0)$ and are used to compute the gradient of $E$. We begin by providing a construction for an orthonormal basis that vanishes at only one point, $s_1$.

1. Generate the full basis for $T_{\gamma_{id}}(\Gamma)$, denoted by $\mathcal{B}$ with elements $b_1, ..., b_m$. This basis is based on gradients of spherical harmonics.
2. Among the basis elements in $\mathcal{B}$, choose two of them, say $b_1$ and $b_2$, such that $\{b_1(s_1), b_2(s_1)\}$ form a basis of $T_{s_1}(\mathbb{S}^2)$.
3. For each basis element $b_i$ other than $b_1$ and $b_2$, replace it by $b_i - (z_1 b_1 + z_2 b_2)$, where scalars $z_1$ and $z_2$ are chosen such that $b_i(s_1) = z_1 b_1(s_1) + z_2 b_2(s_1)$.
4. Remove $b_1$ and $b_2$ from the basis set.
5. The altered vector fields form a basis of the smooth vector fields that vanish at $s_1$.
6. Orthonormalize the remaining basis elements using the Gram-Schmidt procedure under the $\mathbb{L}^2$ metric.

Now, consider that instead of a single point $s_1$, one has $n$ landmark points where the vector fields must vanish. In this case, in Step 2, choose $2n$ basis elements with the property that together, their values at the $n$ points form a basis for the direct sum of the tangent spaces at the $n$ landmark points. The rest of the procedure remains unchanged.

We use a "multi-scale" approach with respect to the landmark-constrained basis. Because the basis is based on gradients of spherical harmonics, we first solve for the optimal parameterization using the lower order spherical harmonics ($b_1, \ldots, b_m$ for a smaller $m$) and continue updating the solution by systematically adding the higher order harmonics (increasing $m$). This allows us to capture more global deformations initially using the lower order harmonics and then update the solution with smaller local changes using the higher order harmonics. We have found that this provides better registration results and it significantly improves the computational time.

### 3.3. Spherical Parameterization

We represent the surface of a given 3D shape with its embedding on a sphere $f : \mathbb{S}^2 \to \mathbb{R}^3$. Genus-0 surfaces can always be embedded in a sphere. In practice, methods such as conformal mapping introduce significant distortions when dealing with complex shapes that contain many elongated parts. Since our framework does not require the mapping to be conformal, we adopt an approach that preserves the mesh details. We implemented the method proposed in [PH03], which progressively embeds a surface on a sphere while minimizing area distortion. We start by reducing the mesh, using progressive mesh simplification, to a basic polyhedra that can be easily embedded on $\mathbb{S}^2$. Then, we iteratively insert vertices and embed each new vertex inside the spherical kernel of its one-ring neighborhood while optimizing for the area distortion. In our implementation, we reconstruct the mesh up to 1500 vertices, which we found sufficient for computing geodesics. This procedure produces spherical maps that preserve important shape features as shown in all of the examples in this paper. Recall that, spherical parameterization of high genus surfaces is still an open problem. Since we are not aiming at solving the parameterization problem, we focus in this paper on genus-0 manifold surfaces.

### 3.4. Landmark detection and correspondence

Unlike previous works that require one-to-one correspondences between the surfaces for computing geodesics, ours requires only the correspondence between few landmarks.

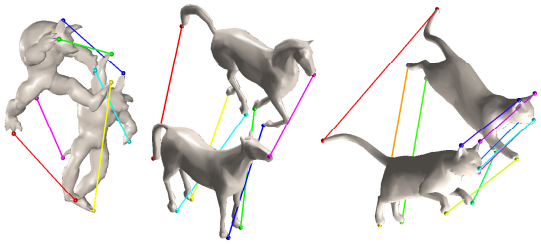

**Figure 3:** *Automatically detected and matched landmarks.*

**Automatic landmark detection.** We use Heat Kernel Signatures (HKS) [SOG09] to detect landmarks that correspond to tips of protrusions of the shapes, which are stable across different poses. The HKS at a point $x$, $h(x) = (h_{t_1}(x,x),\ldots,h_{t_n}(x,x))$, where $h_t(x,y) = \sum_{i=0}^{K} e^{-\lambda_i t}\Phi_i(x)\Phi_i(y)$ is the heat kernel associated with the positive-semidefinite Laplace-Beltrami operator $\Delta_X$, and $\lambda$ and $\Phi$ are the eigenvalues and eigenfunctions of $\Delta_X$. The local maxima of the HKS function for a large time parameter correspond to feature points of interest. The HKS are computed after normalizing the shapes to have total surface area of 1 and use the uniform value of $t = 0.1$ across all shapes. In a final post-processing step, we filter the detected features by keeping one feature point in a neighborhood of size $r$. Fig. 3 shows examples of automatically detected landmarks.

**Landmark correspondences.** When shapes undergo isometric deformations, we use the HKS: for each landmark on the source shape we find $k, k = 3$, candidate correspondences on the target shape. Then, we estimate the best Möbius transform that aligns one surface onto another [LF09]. We randomly sample triplets from the set of landmarks on the source shape. Each pair of triplets, one on the source shape and another from their candidate correspondences on the target shape, votes for a Möbius transform based on the landmark alignment error. In most cases, the transform with the highest vote provides correct landmark correspondences. However, in some cases, symmetric parts are mismatched. Thus, we select the top five configurations, the ones that scored the highest, and manually choose the correct one. Fig. 3 shows some results. When the shapes undergo elastic deformations or contain missing parts, the isometry assumption is no longer valid and the HKS signatures do not provide reliable correspondences. In these cases, while the landmarks can be automatically detected, the correspondences have to be specified manually.

## 4. Results and applications

We demonstrate our framework in the context of three applications. First, we focus on computing geodesics between surfaces that undergo large isometric and elastic deformations and in the presence of missing parts. Second, we demonstrate the usage of the geodesics and geodesic distances in computing shape statistics, i.e, the mean shape of a collection of surfaces. To the best of our knowledge, this is the first time such results are being presented in the graphics community. Finally, we show that our formulation provides a formal measure of the level of asymmetry in a given shape and that it can be used for shape symmeterization. The 3D models used in our experiments are part of the TOSCA [BBK08] and SHREC2007 [GBO07] datasets.

### 4.1. Dense correspondences and geodesics

We present examples of computing one-to-one correspondences, geodesic paths and distances between 3D shapes using the joint Riemannian framework proposed in this paper. We display one-to-one surface correspondences along the geodesic by marking corresponding points with the same color. The visual quality of the geodesic is an important evaluation criterion of the quality of the dense correspondences. Small registration errors will results in significant artifacts and distortions in the intermediate shapes. We include movies of the geodesic deformations for each of the examples as supplementary material.

**Shapes with missing parts.** In Fig. 4-(a), the source and target shapes are similar but the target has a missing finger. Using only a sparse set of landmarks, we are able to obtain natural geodesics that match human intuition. Observe the quality of the intermediate shapes. Note that the quality of the geodesic depends on the quality of the one-to-one correspondence. This observation demonstrates that our approach is able to find good full correspondences between surfaces with missing parts. In Fig. 4-(b) and (c), the legs and tails of the horse and centaur undergo isometric deformations. Some parts are also missing. Our approach deforms the surfaces (using geodesics) into each other in a natural way.

**Isometric deformations.** Fig. 5 shows geodesic paths and distances between surfaces that undergo nearly isometric deformations. Here, the landmarks and initial sparse correspondences are automatically computed and matched as described in Section 3.4. Our framework then simultaneously finds the dense one-to-one correspondences and the geodesic that aligns one shape onto the other. Here we show the computed geodesic and its length, which corresponds to the dissimilarity of the two shapes. Observe again the quality of the intermediate shapes generated by our approach.

**Elastic deformations.** Fig. 6-(a) considers two hands that differ both in pose and in geometry. The geodesic computed with our approach efficiently handles this elastic deformation. The shapes in Fig. 6-(b) differ considerably; the horse is missing its tail, the cow has horns in addition to ears, and the heads are in different poses. Yet, the geodesic computed using our approach handles all of these transformations very well and provides a natural deformation. In Fig. 6-(c) and (d), we consider the surfaces of a horse and a cat, which differ both in geometry and in pose, and a standing horse and

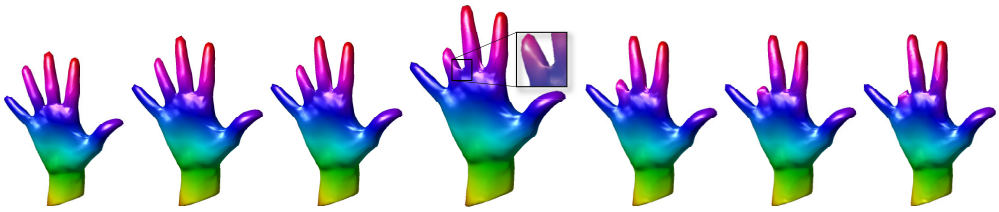

**(a) Hand with missing fingers.** ($L[F^*] = 0.0997$)

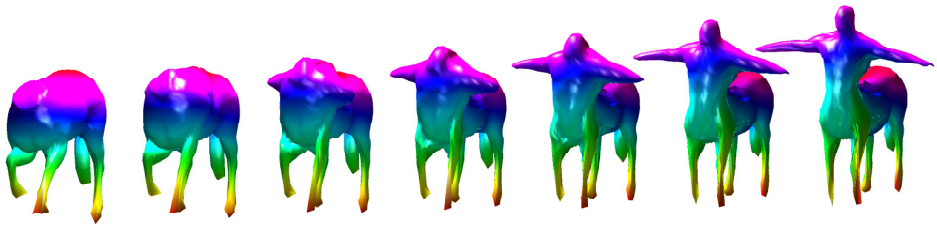

**(b) Headless horse and centaur.** ($L[F^*] = 0.1983$)

**(c) Headless horse and horse.** ($L[F^*] = 0.1977$)

**Figure 4:** *Results on surfaces with missing parts. We show the geodesic between given surfaces and the geodesic distance.*

**(a) Horses undergoing nearly isometric deformations.** ($L[F^*] = 0.1609$)

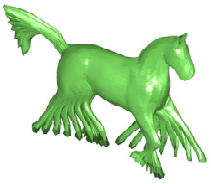

**(c) Two horses.**

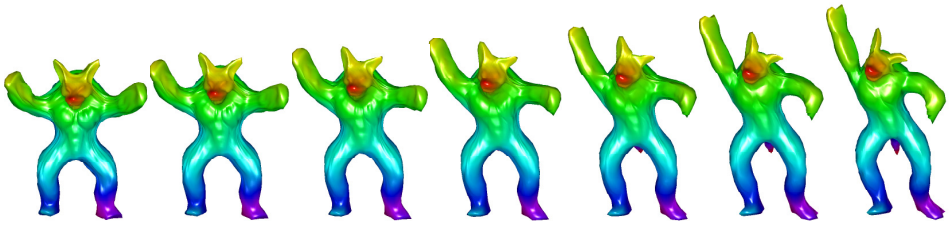

**(b) Armadillo undergoing nearly isometric deformations.** ($L[F^*] = 0.2183$)

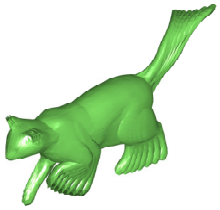

**(d) Two cats.**

**Figure 5:** *Results on surfaces with isometric transformations.*

a laying cat. The transformations in these examples are very drastic and our method is able to handle them very well.

**Evaluation.** First, we quantitatively evaluate the performance of our correspondences and compare them to Blended Intrinsic Maps (BM) [KLF11], Möbius Voting (MV) [LF09], and GMDS [BBK08]. We use all of the centaurs, four cats, two gorillas, and six ant models arbitrarily chosen from the TOSCA [BBK08] and SHREC2007 [GBO07] datasets. The ground-truth correspondences are given and publicly available at [KLF11]. Table 1 summarizes the average error per shape class of each method. We observe that our method performs as well as MV on cats and gorillas, which undergo isometric deformations, and outperforms Blended Intrinsic Maps on the centaur and ant classes. Our approach has the advantage that it can handle large elastic deformations and computes at the same time geodesics, which enables computing shape statistics (see Section 4.2).

Unlike Blended Intrinsic Maps [KLF11], our approach

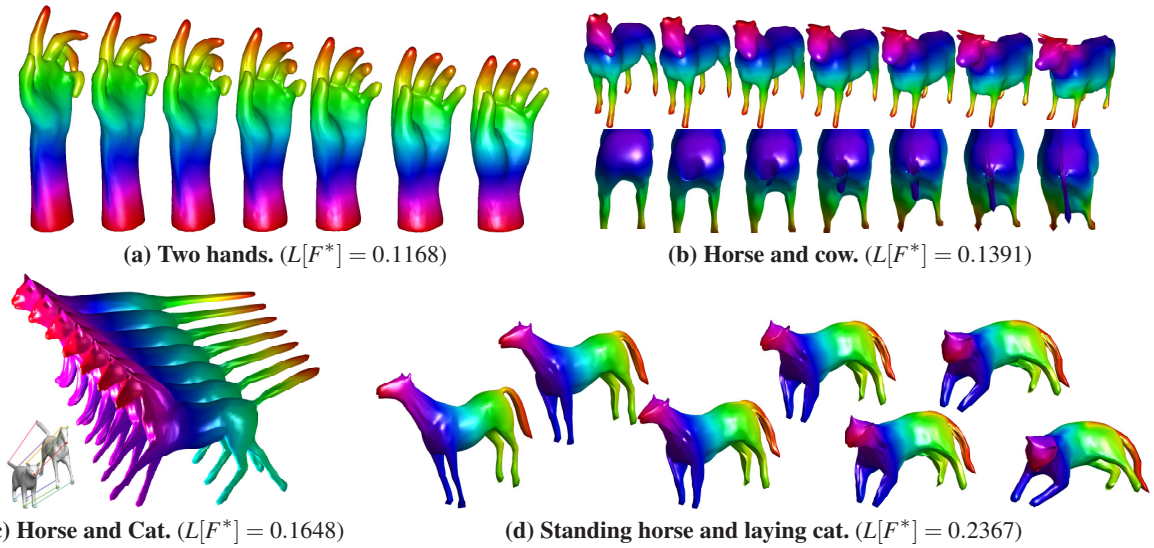

**(a) Two hands.** ($L[F^*] = 0.1168$) **(b) Horse and cow.** ($L[F^*] = 0.1391$)

**(c) Horse and Cat.** ($L[F^*] = 0.1648$) **(d) Standing horse and laying cat.** ($L[F^*] = 0.2367$)

**Figure 6:** *Results on surfaces with elastic deformations.*

also has the advantage that it finds a diffeomorphic mapping. To illustrate the importance of this property and the benefit of our joint framework over methods that solve the two problems separately, we compare the quality of our geodesics to linear interpolations in $\mathbb{R}^3$ between points registered using [KLF11]. We focus on elastic deformations and shapes with missing parts. The results are shown in Fig. 7. Observe that the visual quality of the intermediate shapes generated with our joint approach (Fig. 4-(b)) significantly outperforms the results obtained by solving the correspondence and geodesic problems separately. Finally, previous works that compute geodesics between shapes [KMP06,HRWW12] handled isometric deformations only. In addition, they assumed that a full one-to-one correspondence between the surfaces is given. Our approach handles a wider range of deformations and requires only a sparse set of correspondences (4 to 10 landmarks). The lengths of the geodesics we compute provide a formal distance that measures the difference between shapes of the given surfaces. This quantity is very useful in different applications such as retrieval and classification.

**Timing.** The processing time for solving the joint minimization problem in Eqn. 1 between two spherically parameterized surfaces ($100^2$ vertices) is approximately 580 seconds.

| | #Models | Ours | BM | MV | GMDS |
|---|---|---|---|---|---|
| Centaur | 6 | 0.046 | 0.058 | 0.043 | 0.089 |
| Cat | 4 | 0.056 | 0.034 | 0.083 | 0.149 |
| Gorilla | 2 | 0.050 | 0.019 | 0.021 | 0.091 |
| Ant | 6 | 0.053 | 0.278 | – | – |

**Table 1:** *Average correspondence errors on four classes of shapes that undergo isometric deformations.*

### 4.2. Towards Computation of a Shape Atlas

A shape atlas is a statistical summary and a generative model that capture the essential variability exhibited in a given set of shapes. By summary we mean representations that provide the mean shape and the primary modes of variation in a shape set. These moments – mean and covariance – can also be used to impose generative models on the shape space. In our framework, one can use the geodesic distance in $\mathcal{S}$ defined in Eqn. 1 to compute shape averages or modes of variation of complex surfaces in the presence of fixed landmarks. We illustrate this idea for mean computation next.

Given parameterized surfaces $\{f_1, f_2, \ldots, f_n\} \in \mathcal{F}$ a mean shape is defined as: $[\bar{f}] = argmin_{[f]\in\mathcal{S}} \sum_{i=1}^{n} d([f],[f_i])^2$. We use a gradient-based approach [KKD*11a] to solve this minimization problem. Fig. 8 shows four examples of computing such shape prototypes in our landmark constrained framework. We note that in all of the presented examples the computed mean shape is a natural representative of the given surfaces. The pose of the prototypes is an average of the poses of each of the shapes in the given sample. This is a very intuitive result and it is especially apparent in the example where the body of the average horse is in a neutral pose but its tail is in a pose that is an average of the three given horses. We are not aware of any papers in the graphics literature that compute a proper shape mean (using a formal geodesic distance) on the space of surfaces, using only a sparse set of corresponding landmarks. The ultimate goal in this setup is to derive a full atlas (modes of variation and generative models) and use it to perform comprehensive statistical analysis

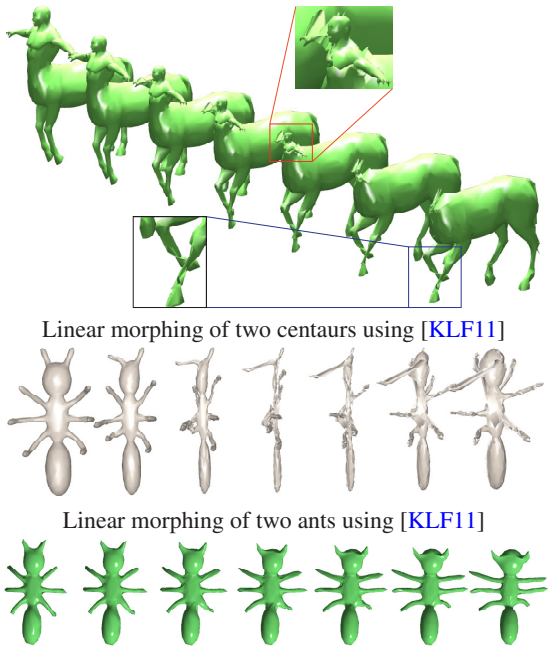


**Figure 7:** *Linear paths computed by independently solving for the correspondence using Blended Intrinsic Maps [KLF11]. Observe the distortions in the intermediate shapes.*

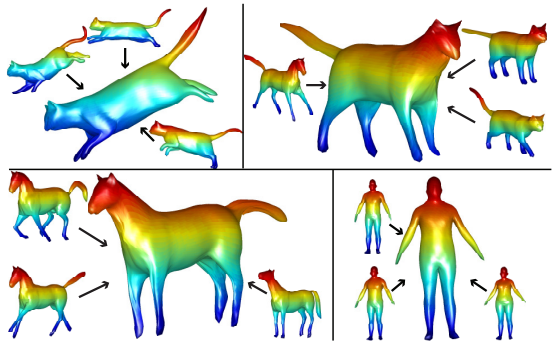

**Figure 8:** *Examples of computing shape averages for three cats in different poses, two cats and a horse in the same pose, three horses in different poses, and three humans with different body shapes.*

of complex surfaces. In addition to mean shapes, one may like to compute median shapes, variability around a mean or median shape using the covariance, perform outlier detection and define statistical models that capture shape variabilities. These models can then be evaluated through random sampling, and clustering or classification studies.

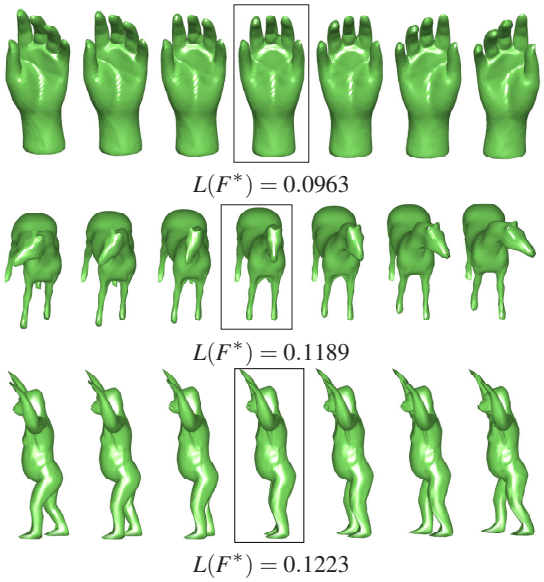


**Figure 9:** *Symmetrizing complex surfaces. Each example shows the geodesic between a surface and its reflection. The midpoint of the geodesic is the nearest symmetric shape. The geodesic distance provides a measure of asymmetry.*

### 4.3. Symmetry Analysis

Symmetry is an important feature of an object and can be useful in many different applications [KS12]. Detection and analysis of symmetry has been studied in literature from different perspectives [MGP07, GAK10]. We take a geometric approach to studying symmetry of complex objects. To analyze the level of symmetry of a surface $f$ using our framework, we first obtain its reflection $\tilde{f} = H(v)f$, where $H(v) = (I - 2\frac{vv^T}{v^Tv})$, for an arbitrary $v \in \mathbb{R}^3$. Let $F^* : [0,1] \mapsto \mathcal{S}$ be the geodesic path between $f$ and $\tilde{f}$. $F^*$ provides valuable information about the symmetry of $f$. First, the length of the path $F^*$ gives a formal measure of asymmetry of $f$. Second, the halfway point along this geodesic, i.e. $F^*(0.5)$, is symmetric. If this geodesic path is unique, then amongst all symmetric shapes, $F^*(0.5)$ is the nearest to $f$ in $\mathcal{S}$. In Fig. 9, we present several examples of symmetrizing highly articulated surfaces. Note that the highlighted midpoints of the presented geodesics are symmetric. These paths provide natural symmetrizations of the given surfaces.

## 5. Summary

We developed a framework for establishing full correspondence and computing geodesics between complex spherical surfaces. An important property of this framework is that the full correspondence and geodesic problems are solved jointly, under the same metric. We presented various results that show the strengths of the proposed framework. In par-

ticular, we demonstrated that it can handle isometric deformations, elastic deformations, and missing parts. While previous works, such as [KMP06, HRWW12] efficiently handled nearly isometric deformations under the assumption that full one-to-one correspondences are given, to the best of our knowledge, this paper is the first work that deals with geodesics in the presence of elastic deformations and using only a sparse set of corresponding landmarks. We proposed a proper metric and demonstrated its utility in various shape analysis applications, such as symmetrization and also the computation of sample statistics, which is a building block towards constructing shape atlases. The results presented in this paper are on genus-0 spherically parameterized surfaces. Our framework however can handle higher genus surfaces if they are parameterized into a common domain. In the future, we plan to test it on other parameter domains. The use of sparse landmarks frees the user from the need of specifying full correspondences, which we believe is a significant progress compared to the state of the art [KMP06,HRWW12]. The use of landmarks is also highly desirable in many applications such as medical imaging or in performance capture. Other applications may prefer fully automatic approaches. An interesting future direction is to study geodesics between meshes over all possible correspondences in the absence of user-specified landmarks. Although at this stage we are able to compute shape average, the ultimate goal in shape analysis is to compute full shape atlases (covariance, etc.) and develop generative models of shapes. This paper is a big step toward this ultimate goal.

**Acknowledgement.** This work is supported by NSF DMS-0915003 and NSF DMS- 1208959 grants. H. Laga is supported by the South Australian State Government through its Premier's Science and Research Fund.

## References

[ACP03] ALLEN B., CURLESS B., POPOVIC Z.: The space of human body shapes. *ACM TOG 22* (2003), 587 – 594. 1

[BBK08] BRONSTEIN A. M., BRONSTEIN M. M., KIMMEL R.: *Numerical Geomertry of Non-Rigid Shapes*. Springer, 2008. 6, 7

[BGK95] BRECHBÜHLER C., GERIG G., KÜBLER O.: Parameterization of closed surfaces for 3D shape description. *CVIU 61*, 2 (1995), 154–170. 2

[GAK10] GHOSH D., AMENTA N., KAZHDAN M.: Closed-form blending of local symmetries. *CGF* (2010), 1681–1688. 9

[GBO07] GIROGI D., BIASOTTI S., OARABOSCHI L.: Shape retrieval contest 2007: Watertight models track. In *CGF* (2007). 6, 7

[GVM04] GLAUNÈS J., VAILLANT M., MILLER M.: Landmark matching via large deformation diffeomorphisms on the sphere. *JMIV 20* (2004), 179–200. 4

[HRWW12] HEEREN B., RUMPF M., WARDETZKY M., WIRTH B.: Time-discrete geodesics in the space of shells. *CGF 31*, 5 (2012). 2, 3, 8, 10

[KKD*11a] KURTEK S., KLASSEN E., DING Z., AVISON M., SRIVASTAVA A.: Parameterization-invariant shape statistics and probabilistic classification of anatomical surfaces. In *Information Processing in Medical Imaging* (2011), pp. 147–158. 8

[KKD*11b] KURTEK S., KLASSEN E., DING Z., JACOBSON S., JACOBSON J., AVISON M., SRIVASTAVA A.: Parameterization-invariant shape comparisons of anatomical surfaces. *IEEE TMI 30*, 3 (2011), 849–858. 2, 3

[KKDS10] KURTEK S., KLASSEN E., DING Z., SRIVASTAVA A.: A novel Riemannian framework for shape analysis of 3D objects. In *IEEE CVPR* (2010). 3

[KKG*12] KURTEK S., KLASSEN E., GORE J. C., DING Z., SRIVASTAVA A.: Elastic geodesic paths in shape space of parameterized surfaces. *IEEE TPAMI 34*, 9 (Sept. 2012), 1717–1730. 2, 3, 4

[KLF11] KIM V. G., LIPMAN Y., FUNKHOUSER T.: Blended intrinsic maps. *ACM TOG 30* (2011), 79:1–79:12. 2, 7, 8, 9

[KMP06] KILIAN M., MITRA N. J., POTTMANN H.: Geometric modeling in shape space. In *SIGGRAPH* (2006). 2, 3, 8, 10

[KS04] KRAEVOY V., SHEFFER A.: Cross-parameterization and compatible remeshing of 3D models. *ACM TOG 23*, 3 (Aug. 2004), 861–869. 2

[KS12] KURTEK S., SRIVASTAVA A.: Elastic symmetry analysis of anatomical structures. In *Mathematical Methods in Biomedical Image Analysis* (2012), pp. 33–38. 9

[LF09] LIPMAN Y., FUNKHOUSER T.: Mobius voting for surface correspondence. *ACM TOG 28* (2009), 72:1–72:12. 2, 6, 7

[MGP07] MITRA N., GUIBAS L., PAULY M.: Symmetrization. *ACM TOG 26*, 3 (2007). 9

[OLGM11] OVSJANIKOV M., LI W., GUIBAS L., MITRA N. J.: Exploring the continuous variability in collections of 3D shapes. *ACM TOG 30* (2011), 33:1–33:10. 1

[PH03] PRAUN E., HOPPE H.: Spherical parameterization and remeshing. *ACM TOG 22*, 3 (2003), 340–349. 3, 5

[SKJJ11] SRIVASTAVA A., KLASSEN E., JOSHI S., JERMYN I.: Shape analysis of elastic curves in euclidean spaces. *IEEE TPAMI 33*, 7 (2011), 1415–1428. 2, 4

[SOG09] SUN J., OVSJANIKOV M., GUIBAS L.: A concise and provably informative multi-scale signature based on heat diffusion. In *SGP* (2009), pp. 1383–1392. 6

[vKZHCO10] VAN KAICK O., ZHANG H., HAMARNEH G., COHEN-OR D.: A survey on shape correspondence. In *Eurographics State-of-the-art Report* (2010). 2

[WSSC11a] WINDHEUSER T., SCHLICKEWEI U., SCHMIDT F. R., CREMERS D.: Geometrically consistent elastic matching of 3D shapes: A linear programming solution. In *ICCV* (2011). 2

[WSSC11b] WINDHEUSER T., SCHLICKEWEI U., SCHMIDT F. R., CREMERS D.: Large-scale integer linear programming for orientation-preserving 3D shape matching. In *CGF* (2011). 2

[YMS*08] YOUNES L., MICHOR P. W., SHAH J., MUMFORD D., LINCEI R.: A metric on shape space with explicit geodesics. *Matematica E Applicazioni 19*, 1 (2008), 25–57. 2

[YYPM11] YANG Y.-L., YANG Y.-J., POTTMAN H., MITRA N.: Shape space exploration of constrained meshes. *ACM TOG 30* (2011), 124:1–124:12. 1

[ZSCO*08] ZHANG H., SHEFFER A., COHEN-OR D., ZHOU Q., VAN KAICK O., TAGLIASACCHI A.: Deformation-driven shape correspondence. In *SGP* (2008), pp. 1431–1439. 2

[ZWW*10] ZENG Y., WANG C., WANG Y., GU X., SAMARAS D., PARAGIOS N.: Dense non-rigid surface registration using high-order graph matching. In *CVPR* (2010), pp. 382 –389. 2